Available online at www.sciencedirect.com
SCIENCE DIRECT®
Journal of Molecular Catalysis A: Chemical 212 (2004) 291–300
JOURNAL OF MOLECULAR CATALYSIS A: CHEMICAL
www.elsevier.com/locate/molcata

The application of $\{(DMF)_{10}Yb_2[TM(CN)_4]_3\}_\infty$ (TM = Ni, Pd) supported on silica to promote gas phase phenol hydrogenation

Sheldon G. Shore [a], Errun Ding [a], Colin Park [b,1], Mark A. Keane [b,*]

[a] *Department of Chemistry, The Ohio State University, Columbus, OH 43210-1185, USA*
[b] *Department of Chemical & Materials Engineering, University of Kentucky, Lexington, KY 40506 0046, USA*

Received 16 October 2003; received in revised form 6 November 2003; accepted 7 November 2003

Abstract

The catalytic gas phase phenol hydrogenation activities/selectivities associated with Pd/SiO_2 prepared by $Pd(NO_3)_2$ and $Pd(C_2H_3O_2)_2$ impregnation have been compared with those delivered by $Pd–Yb/SiO_2$ prepared from a $\{(DMF)_{10}Yb_2[Pd(CN)_4]_3\}_\infty$ precursor. The Pd metal loading spanned the range 1–10% (w/w) and the reaction was conducted over the temperature interval 398–448 K. Phenol hydrogenation yielded both cyclohexanone as a partially hydrogenated reactive intermediate and cyclohexanol as the fully hydrogenated product. The activated catalysts have been characterized by HRTEM/EDX, XPS and XRD. The reaction exhibits a slight dependence on Pd particle size with a lower specific hydrogenation activity associated with larger Pd particles. The incorporation of Yb resulted in an appreciable enhancement of phenol conversion. Yb/SiO_2, however, did not exhibit any hydrogenation activity and the promotional effect of Yb in $Pd–Yb/SiO_2$ is tentatively attributed to hydrogen transfer via surface Yb hydride. The effect of contact time and reaction temperature on activity/selectivity has been considered and is discussed in terms of phenol/catalyst interaction(s). The promotional effect of Yb also extends to phenol hydrogenation over supported Ni (5%, w/w Ni) where $Ni–Yb/SiO_2$ delivered higher conversions and higher overall cyclohexanone yields when compared with Ni/SiO_2.
© 2003 Elsevier B.V. All rights reserved.

Keywords: Phenol hydrogenation; Silica supported Pd/Yb and Ni/Yb; Cyclohexanone; Cyclohexanol; Selective hydrogenation

1. Introduction

Phenol hydrogenation can proceed in a stepwise fashion with cyclohexanone as the partially hydrogenated and cyclohexanol the fully hydrogenated products. The selective hydrogenation to cyclohexanone is of commercial significance as a viable synthetic route to a key raw material in the production of caprolactam for nylon 6 and adipic acid for nylon 66 [1]. The alternative route, oxidation of cyclohexane requires high temperatures and pressures and generates appreciable by-products that lower cyclohexanone yield and complicate the recovery/separation steps. Supported Pd has thus far been the predominant catalytic agent used to promote phenol hydrogenation in both gas [2–11] and liquid [12,13] phase operation. The use of Ni-based catalysts has, by comparison, received less attention [14–18]. Reaction selectivity, in terms of cyclohexanone production, is strongly dependent on reaction conditions [9,10,16,19] and selectivities in excess of 95% have been quoted in the literature [2,7,10,14,15]. However, in the sequential hydrogenation of phenol, cyclohexanone selectivity is inextricably linked to fractional phenol conversion and the higher the conversion the greater is the likelihood of complete hydrogenation to cyclohexanol. The attainment of a high cyclohexanone selectivity (>95%) at elevated conversions (>80%) remains a challenging catalysis problem. The latter can only be solved by establishing a direct correlation between activity/selectivity and catalyst surface structure/properties. Recent findings have highlighted the respective roles of metal loading [2,3,5,8,14,16,20], acid-base support properties [2,3,9,19] and the incorporation of promoters such as alkali [3,11,21] and alkaline [11,21] metals in modifying phenol/catalyst interaction(s) and governing the ultimate product composition. The results generated in this study are compared with the pertinent trends that have emerged from the literature.

* Corresponding author. Tel.: +1-859-257-5857; fax: +1-859-323-1929.
E-mail address: makeane@engr.uky.edu (M.A. Keane).
[1] Present address: Synetix, Billingham, Cleveland TS23 1LB, UK.

1381-1169/$ – see front matter © 2003 Elsevier B.V. All rights reserved.
doi:10.1016/j.molcata.2003.11.004

In an earlier communication [22], we demonstrated that a silica supported Pd–Yb bimetallic catalyst, derived from a cyanide bridged lanthanide-palladium complex ($\{(DMF)_{10}Yb_2[Pd(CN)_4]_3\}_\infty$), exhibited quite distinct phenol hydrogenation behavior when compared with monometallic Pd catalysts prepared from conventional nitrate and acetate salt precursors. This was manifest in appreciably higher phenol conversions over the bimetallic, an effect that we initially ascribed to possible electron donation from Yb that serves to enhance the intrinsic hydrogenation activity of the Pd sites. The earlier communication was limited to a single Pd loading (5% w/w) and one reaction temperature (423 K): the Pd–Yb stoichiometry in the bimetallic system = 3/2. We have since extended the work to consider two additional Pd loadings (1% and 10%, w/w Pd) with reaction over the range 398–448 K and report herein the results of these additional studies. In addition, we have obtained supplementary catalyst characterization data (TEM, XRD and XPS) and have extended the study to consider the influence of Yb on the phenol hydrogenation activity/selectivity of silica supported Ni.

2. Experimental

2.1. Catalyst preparation, activation and characterization

The transition metal (TM) complex $\{(DMF)_{10}Yb_2[TM(CN)_4]_3\}_\infty$, where TM = Pd or Ni, was prepared using a procedure previously described by Shore and co-workers [23]. The solution was contacted with a sample of fumed SiO_2 (Aldrich, surface area >200 $m^2\,g^{-1}$) to deliver three Pd (1, 5, and 10%, w/w) and one Ni (5%, w/w) loading. The DMF was removed from the impregnated SiO_2 under vacuum over a period of 12 h at room temperature. The resulting white solid was loaded in a quartz boat, placed in a furnace, flushed with H_2 for ca. 10 min and reduced under a steady H_2 flow with incremental temperature increases of 25 K, approximately every 10 min, to a final temperature of 523 K which was maintained for 30 min. The sample was then flushed in He and passivated in a 1% (v/v) O_2 in He flow at room temperature. Samples of 1, 5, and 10% (w/w) Pd and 5% (w/w) Ni on SiO_2 were prepared employing the metal acetate dissolved in DMF as precursor. The same fumed SiO_2 was contacted with the acetate precursor and activated/passivated as above. For comparative purposes, 1, 5, and 10% (w/w) Pd/SiO_2 and 5% (w/w) Ni/SiO_2 were prepared by impregnation of the same fumed silica with 2-butanolic solutions of $Pd(NO_3)_2$ or $Ni(NO_3)_2$. A 5% (w/w) Yb on SiO_2 was also prepared where weighed amounts of SiO_2 and Yb powder were charged into a reaction flask in a drybox. Liquid ammonia was then vacuum-transferred into this flask at 195 K, the mixture was stirred for ca. 3 h and the liquid ammonia was then pumped away. Each sample was sieved (ATM fine test sieves) into batches of 75 μm average particle diameter. The metal loadings were determined (to within ± 2%) by inductively coupled plasma-optical emission spectrometery (ICP-OES, Vista-PRO, Varian Inc.) from the diluted extract of aqua regia.

High resolution transmission electron microscopy (HRTEM) analysis was carried out using a Philips CM200 FEGTEM microscope equipped with a UTW energy dispersive X-ray (EDX) detector (Oxford Instruments) and operated at an accelerating voltage of 200 kV. The specimens were prepared by ultrasonic dispersion in 2-butanol, evaporating a drop of the resultant suspension onto a holey carbon support grid. The Pd particle size distribution profiles (and mean Pd sizes) presented in this study are based on a measurement of over 500 individual particles. The specific Pd surface area (S_{Pd}, $m^2\,g_{Pd}{}^{-1}$) was calculated from the relationship [24]

$$S_{Pd} = \frac{6}{\rho d_{Pd}} \quad (1)$$

where d_{Pd} is the mean particle size and ρ is the Pd specific mass (11.97 g cm^{-3}): d_{Pd} was obtained from

$$d_{Pd} = \frac{\sum_i n_i d_i}{\sum_i n_i} \quad (2)$$

where n_i is the number of Pd particles of diameter d_i and $\sum_i n_i > 500$. A secondary ion mass spectrometric analysis (SIMS, VG ESCALAB) of each activated catalyst (pressed into indium foil) revealed only the presence of Si, Pd or Ni and (in the case of the supported bimetallics) Yb on the surface. X-ray powder data were collected on a Bruker D8 Advance X-ray powder diffractometer (Cu Kα radiation) from activated/passivated samples that were loaded in 0.5 mm Lindeman glass capillaries in a glove box and sealed. X-ray photoelectron spectroscopic (XPS) analyses were conducted using a Kratos Axis Ultra spectrometer with monochromatized Mg Kα radiation (1253.6 eV). A sample of activated/passivated catalyst was adhered to a conducting carbon tape, mounted in the sample holder and subjected to UHV conditions (~1.3×10^{-7} Pa) overnight prior to analysis. Full range surveys (0–1000 eV) and high resolution spectra (range of ~30 eV) of Pd $3d_{5/2}$, Yb $4d_{5/2}$, Si 2p, O 1s and C 1s were collected. The C 1s peak, centred at 284.5 eV served as reference to calibrate the binding energy values. The signals for Pd and Yb were much weaker than Si and O, due to the low concentrations in the SiO_2 matrix with the result that extended scans were employed to improve the signal–noise ratio.

2.2. Catalytic reactor system

Prior to reaction, each catalyst sample was activated (10 K min^{-1} in 60 $cm^3\,min^{-1}$ dry H_2) in situ under atmospheric pressure in a fixed bed glass reactor (i.d. = 15 mm) at 523 K (in the case of Pd and Pd–Yb) and 673 K (in the case of Ni and Ni/Yb). The catalytic reactor approximated

plug flow pattern and has been fully described previously [2,16] but some details, pertinent to this study, are given below. A Model 100 (kd Scientific) microprocessor controlled infusion pump was used to deliver an aqueous solution of phenol at a fixed calibrated flow rate, carried through the catalyst bed in a stream of dry H_2. The phenol molar feed rate was varied from 5.2×10^{-4} to $9.4 \times 10^{-3}\,h^{-1}$ in order to test adherence to pseudo-first order kinetics where H_2 was maintained at least twelve times in excess of stoichiometric quantities; the gas space velocity was kept constant at $3620\,h^{-1}$. The catalyst was supported on a glass frit and a layer of glass beads above the catalyst bed served as a pre-heating zone to ensure that the reactants were vaporized and reached the reaction temperature (398–448 K) before contacting the catalyst. The reactor was operated, using the criteria outlined elsewhere [25], with negligible internal or external diffusion retardation of reaction rate (effectiveness factor >0.99). Heat transport effects can also be disregarded when applying the criteria set down by Mears [26]; the temperature differential between the catalyst particles and bulk fluid phase was <1 K. Repeated catalytic runs generated results that were reproducible to within ±7%. The reactor effluent was frozen in a liquid nitrogen trap for subsequent analysis which was made using an AI Cambridge GC94 chromatograph equipped with a flame ionization detector and employing a DB-150 m × 0.20 mm i.d., 0.33 μm capillary column (J&W Scientific), as described elsewhere [7]. Quantitative analysis was based on relative peak area with acetone as solvent where analytical repeatability was better than ±0.1% and the detection limit corresponded to a phenol conversion less than 0.1 mol%. The overall fractional conversion of phenol (x_{phenol}) is given by

$$x_{phenol} = \frac{[C_6H_5OH]_{in} - [C_6H_5OH]_{out}}{[C_6H_5OH]_{in}} \quad (3)$$

while reaction selectivity (as a percentage) in terms of cyclohexanone formation ($S_{C=O}$) can be represented by

$$S_{C=O} = \frac{[C_6H_{10}O]_{out}}{[C_6H_5OH]_{in} - [C_6H_5OH]_{out}} \times 100 \quad (4)$$

and percentage cyclohexanone yield ($Y_{C=O}$ %) is given by

$$Y_{C=O} = \frac{[C_6H_{10}O]_{out}}{[C_6H_5OH]_{in}} \times 100 \quad (5)$$

where [] denotes concentration, and in and out refer to the organic entering and exiting the reactor. All the reactants were Analar grade and were used without further purification.

3. Results and discussion

The Pd-based catalysts considered in this study are listed in Table 1, which includes the mean Pd particle sizes derived from TEM analyses. The activated monometallic Pd catalysts derived from the nitrate and acetate precursors are denoted A/B/C and I/II/III, respectively. The mean Pd diameter was found to increase with increasing Pd loading for the three catalyst families. This is well illustrated by the TEM generated Pd size distribution histograms shown in Fig. 1 where a broadening of the size distribution and overall shift to higher values is evident at higher Pd loadings. It is instructive to note that the Pd particle size in the Pd–Yb/SiO_2 bimetallic catalysts was less sensitive to metal loading and the size distribution profiles are similar at each loading (Fig. 1c). The nature of the Pd metal dispersion in these catalysts can be assessed from the representative TEM images presented in Fig. 2. As a general observation, the Pd particles in both monometallic catalysts are characterized by a rounded morphology whereas a significant proportion of the Pd particles in the Pd–Yb/SiO_2 sample adopted more faceted shapes, indicative of subtle changes in the metal/support interaction(s). The EDX analyses, reported previously [22], revealed a thin coating of Yb spread over the catalysts surface with no evidence of any distinct clustering or particles of Yb in the Pd–Yb/SiO_2 samples. Representative X-ray powder patterns of monometallic Pd/SiO_2 and Yb/SiO_2 and bimetallic Pd–Yb/SiO_2 are shown in Fig. 3. The diffraction pattern for Yb/SiO_2 did not reveal the presence of crystalline Yb or a known hydride of ytterbium. However, there is evidence (indicated in Fig. 3) of crystalline $Yb(NH_2)_3$

Table 1
Effect of Pd precursor and presence of Yb on the mean Pd particle diameter (d) obtained from TEM analysis and the associated specific phenol hydrogenation pseudo-first order rate constants (k): $T = 448$ K

Catalyst	Pd precursor	Pd (%, w/w)	d (nm)	k ($\times 10^5$(mol h^{-1} (m^2 g_{Pd}^{-1})$^{-1}$)
Pd/SiO_2-A	$Pd(NO_3)_2$	1	1.9	3.1
Pd/SiO_2-I	$Pd(C_2H_3O_2)_2$	1	3.4	2.5
Pd–Yb/SiO_2-I	$\{(DMF)_{10}Yb_2[Pd(CN)_4]_3\}_\infty$	1	5.0	5.7
Pd/SiO_2-B	$Pd(NO_3)_2$	5	5.2	2.3
Pd/SiO_2-II	$Pd(C_2H_3O_2)_2$	5	6.0	2.0
Pd–Yb/SiO_2-II	$\{(DMF)_{10}Yb_2[Pd(CN)_4]_3\}_\infty$	5	5.1	5.4
Pd/SiO_2-C	$Pd(NO_3)_2$	10	8.3	2.4
Pd/SiO_2-III	$Pd(C_2H_3O_2)_2$	10	7.4	1.8
Pd–Yb/SiO_2-III	$\{(DMF)_{10}Yb_2[Pd(CN)_4]_3\}_\infty$	10	6.3	4.9

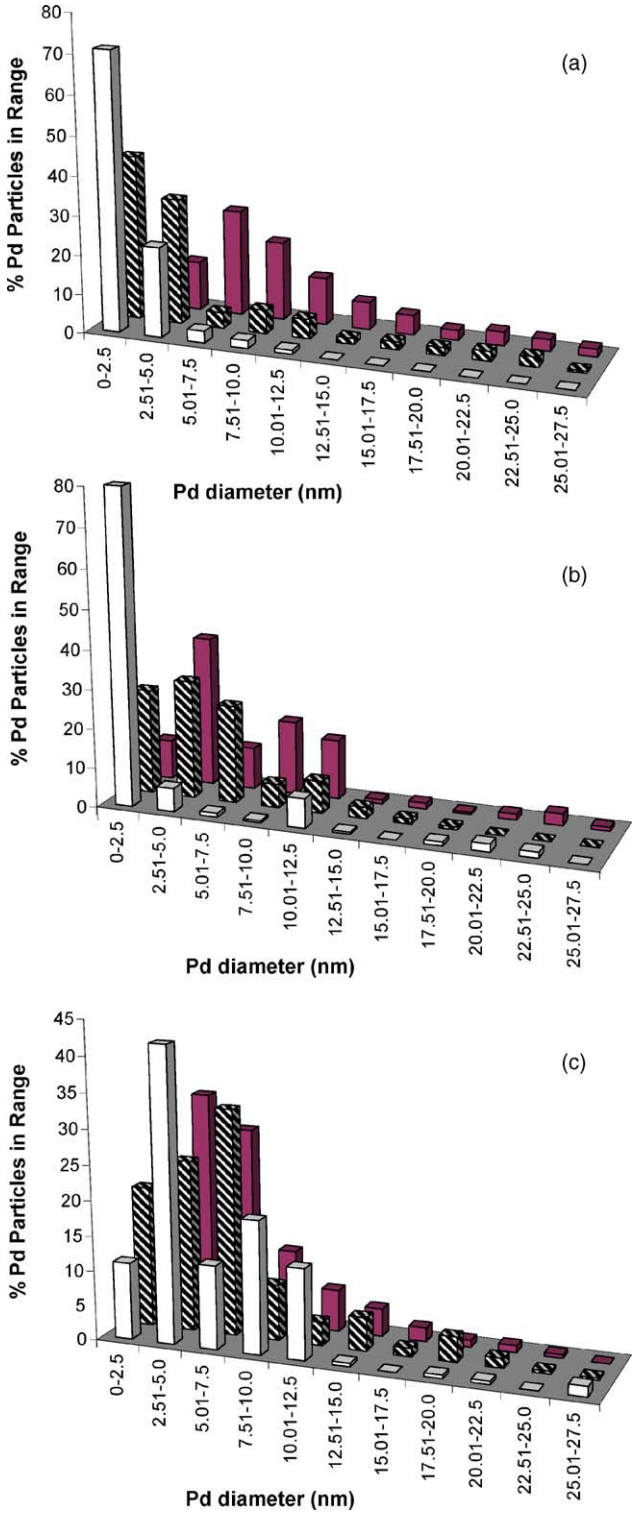

Fig. 1. Palladium particle size distribution associated with activated 1% (w/w) (open bars), 5% (w/w) (hatched bars), 10% (w/w) (solid bars) Pd loadings: (a) Pd/SiO_2 (A, B, and C) derived from the $Pd(NO_3)_2$ precursor; (b) Pd/SiO_2 (I, II, and III) derived from the $Pd(C_2H_3O_2)_2$ precursor; (c) $Pd–Yb/SiO_2$ (I, II, and III) derived from the $\{(DMF)_{10}Yb_2[Pd(CN)_4]_3\}_\infty$ precursor.

and $Yb(NH_2)_2$ [27] in addition to some unidentified species. The X-ray powder pattern associated with Pd/SiO_2 is consistent with an exclusive cubic symmetry where the d spacings (2.24801, 1.94622, 1.37579, 1.17231, 1.12192, and 1.00515 Å) and relative intensities are in excellent agreement with those reported by Kern and Eysel [28]. The pattern for the Pd–Yb bimetallic revealed only the presence of crystalline Pd species, an observation that is in keeping with the TEM-EDX detection of Yb as a surface film. The broad character of Pd diffraction maxima in $Pd–Yb/SiO_2$ suggests short range order. It should be noted that extended exposure of this sample to H_2 has generated a pattern with sharper maxima.

Cyclohexanone and cyclohexanol were the only observed reaction products in the gas phase transformation of aqueous phenol solutions over each silica supported Pd and Pd–Yb catalyst. At temperatures in excess of ca. 473 K there was evidence of benzene formation (hydrodehydroxylation) that was more significant over the higher Pd loaded catalysts and which was further promoted at $T > 473$ K. In preliminary studies, the transformation of methanolic phenol solutions yielded anisole as a major product, formed through a catalyzed methylation step. The catalytic study was accordingly limited to an aqueous phenol feed to the reactor (with vaporization prior to reaction) at temperatures less than 473 K in order to assess the intrinsic hydrogenation activity of these catalysts. There was no detectable condensation to form dicyclohexylether, as has been reported for Pd on acidic supports [3,9]. The product composition associated with the monometallic Pd/SiO_2 was largely independent of time-on-stream whereas the $Pd–Yb/SiO_2$ catalysts were characterized by distinct short range temporal variations in terms of activity/selectivity. The latter is illustrated in Fig. 4 where the fractional phenol conversion over the Pd–Yb system can be seen to decrease with a concommitant increase in cyclohexanone selectivity at $\Delta t < 2$ h but steady state activity/selectivity is ultimately attained. The anti-sympathetic relationship between x_{phenol} and $S_{C=O}$ is to be expected in a sequential hydrogenation scheme where complete hydrogenation should be enhanced at higher x_{phenol}. In marked contrast, phenol conversion/cyclohexanone selectivity over both Pd/SiO_2 catalysts was essentially time invariant. All the catalytic data quoted from this point on refer to steady state conversions.

We have shown elsewhere that phenol hydrogenation kinetics can be adequately represented using a standard pseudo-first order treatment [16,22]. This can be tested by integrating the design equation for a plug flow reactor where pseudo-first order dependence will yield a straight line plot relating fractional conversion (x_{phenol}) to W/F_{phenol} (catalyst weight to phenol molar flow rate ratio) according to

$$\ln\left(\frac{1}{1-x_{phenol}}\right) = k\frac{W}{F_{phenol}} \quad (6)$$

Three representative plots are given in Fig. 5 where it is clear (correlation coefficient >0.995) that the pseudo-first order

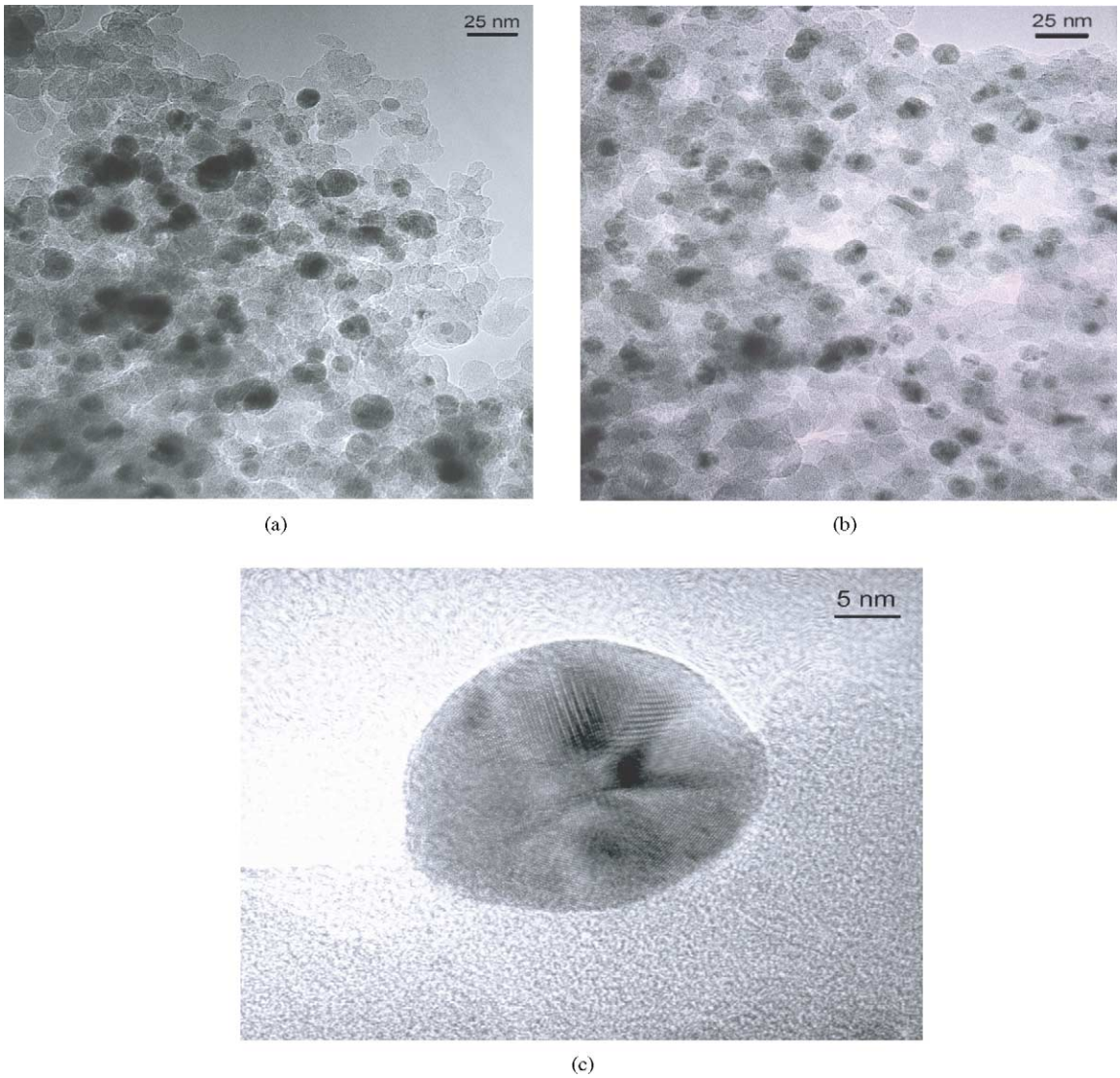

Fig. 2. Representative low resolution TEM images of (a) Pd/SiO_2-B, (b) Pd–Yb/SiO_2-II, and (c) HRTEM of an isolated larger Pd particle in Pd–Yb/SiO_2-I.

treatment holds. A least-squares fit, forced to go through the origin, was used to determine rate constants that were converted to specific values using Eq. (1) and are recorded in Table 1. Taking each catalyst family in turn, the specific rate constant is lower for the higher Pd loadings/larger Pd particle sizes, albeit the dependence is slight. This observation is largely in keeping with earlier work that suggested an invariant specific rate where the average Pd particle size (on MgO) exceeded ca. 2 nm [2,8]. One significant feature is the appreciably higher hydrogenation rates associated with the Pd–Yb bimetallic system that extends over the entire range of Pd loadings. It has been shown elsewhere [20] that the d-character of supported Pd governs, to a great extent, phenol hydrogenation activity where electron deficient Pd sites exhibit a lower inherent rate of phenol consumption. The higher specific rate constants associated with Pd–Yb/SiO_2 may then be linked to electron donation from the strongly electropositive lanthanide metal, possibly facilitated through the intimate association of the Yb film with the supported Pd particles. The latter can be probed by XPS analysis and representative spectra for a silica supported Pd and Pd–Yb are given in Fig. 6 over the binding energy range 332–341 eV wherein two peaks arise that can be positively assigned to Pd $3d_{5/2}$ and Pd $3d_{3/2}$. Focusing on the Pd $3d_{5/2}$ signal, the extracted binding energy of 334.4 eV for Pd/SiO_2-II is in excellent agreement with that recorded elsewhere for Pd/MgO [7]. The XPS spectrum for the Pd–Yb bimetallic over the same range of binding energies is essentially equivalent and the shift of the Pd $3d_{3/2}$ peak by 0.2 eV to 334.2 eV may be suggestive of some slight increase in electron density at the Pd sites. This difference in XPS response is, however, negligible and the observed enhancement of phenol hydrogenation due to Yb inclusion can not then be attributed to electronic effects.

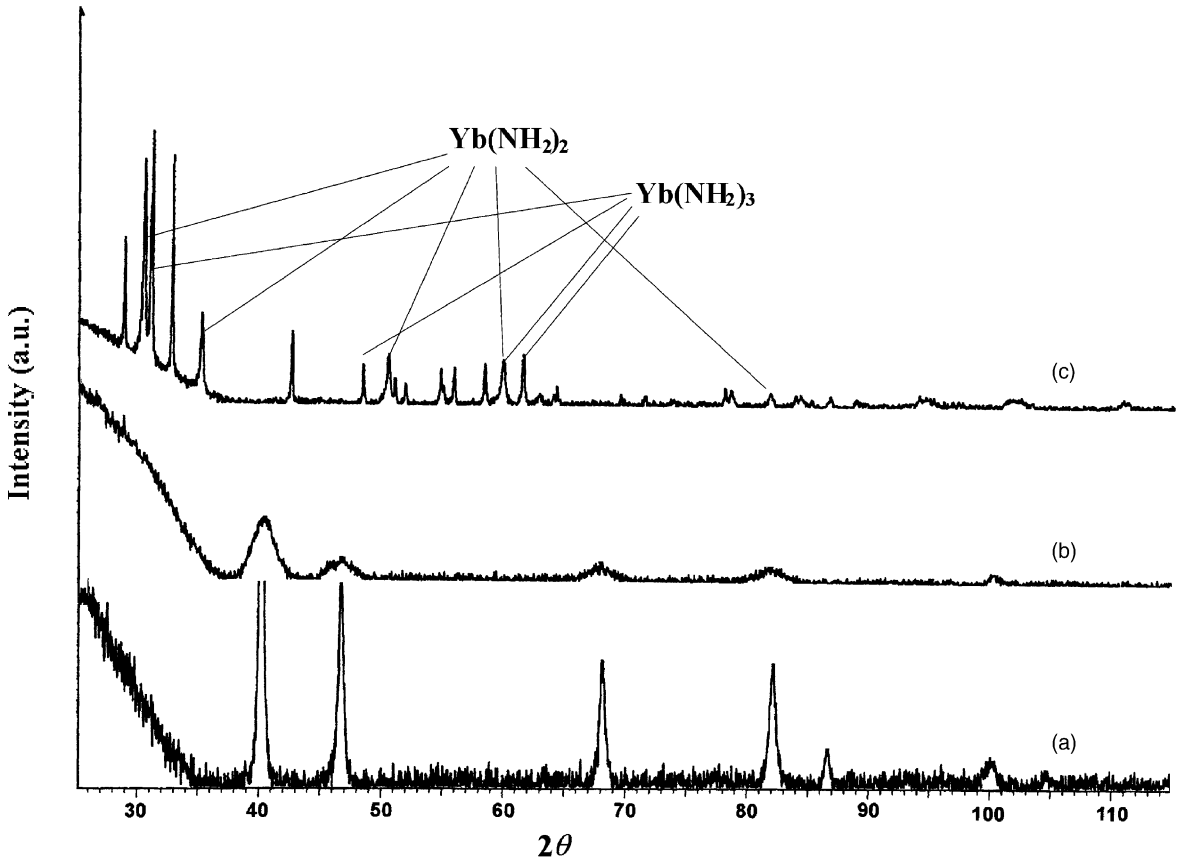

Fig. 3. XRD patterns associated with (a) Pd/SiO_2-II, (b) $Pd–Yb/SiO_2$-II, and (c) Yb/SiO_2 with peak assignments for $Yb(NH_2)_2$ and $Yb(NH_2)_3$.

While there is a dearth of literature on Pd–Yb catalyst systems, there is, however, evidence [29] that alloying Pd with lanthanides has an appreciable impact on hydrogen adsorption behavior. Ytterbium is known to form a dihydride by reaction with hydrogen at room temperature and atmospheric pressure [30–32]. The formation of higher hydrides is possible at higher temperatures and elevated pressure [33] with a switch from an orthorhombic to a face-centered cubic structure at temperatures in excess of 673 K [34]. Imamura et al., in studying silica supported Pd–Yb prepared by the reaction of Pd/SiO_2 with Yb dissolved in liquid ammonia, have reported that the presence of Yb served to generate a higher concentration of surface active hydrogen [35] with a subsequent enhancement of propene [36] and propyne [37] hydrogenation rates. Our bimetallic synthesis strategy differs from that of Imamura et al. in that we introduce both Pd and Yb simultaneously to the support ($\{(DMF)_{10}Yb_2[Pd(CN)_4]_3\}_\infty$ precursor) as opposed to a stepwise addition. Our one step synthetic route should favor a more intimate and uniform interaction of both metals on the silica support. The Yb/SiO_2 sample did not exhibit any hydrogenation activity under the same reaction conditions. The enhanced hydrogenation over $Pd–Yb/SiO_2$ is clearly a synergetic effect where the Yb component may act as a source of surface hydrogen via the hydride. It has been shown [38] that the hydrogen associated with Yb-H films is highly mobile with hydrogen release at elevated temperatures. We have now initiated a program of catalyst characterization involving in situ XRD and H_2 chemisorption/TPD to establish and quantify the surface hydride species and hydrogen uptake/release characteristics of $Pd–Yb/SiO_2$ under reaction conditions.

The relationship between fractional conversion of phenol and cyclohexanone selectivity ($S_{C=O}$) where temperature was kept constant and the W/F_{phenol} parameter varied is shown in Fig. 7. The parameter W/F_{phenol} (units, g h mol^{-1}) has the physical significance of contact time. In every instance, higher conversions (corresponding to higher W/F_{phenol} values) favored complete hydrogenation to the alcohol. The selectivity profiles coincided for both families of Pd/SiO_2 regardless of Pd loading while complete hydrogenation was preferred over the $Pd–Yb/SiO_2$ systems at each x_{phenol}, illustrating the intrinsically grater hydrogenation capability of the supported bimetallic. The effect of reaction temperature on phenol hydrogenation activity can be assessed from the entries in Fig. 8 wherein the fractional conversion of phenol (x) relative to that at 398 K (x_{398K}) is plotted as a function of temperature. In every instance the steady state phenol conversion decreased over the temperature interval $398\,K \leq T \leq 448\,K$. A drop in phenol conversion with increasing temperature has been reported previously [3,8–10,15] and has been attributed

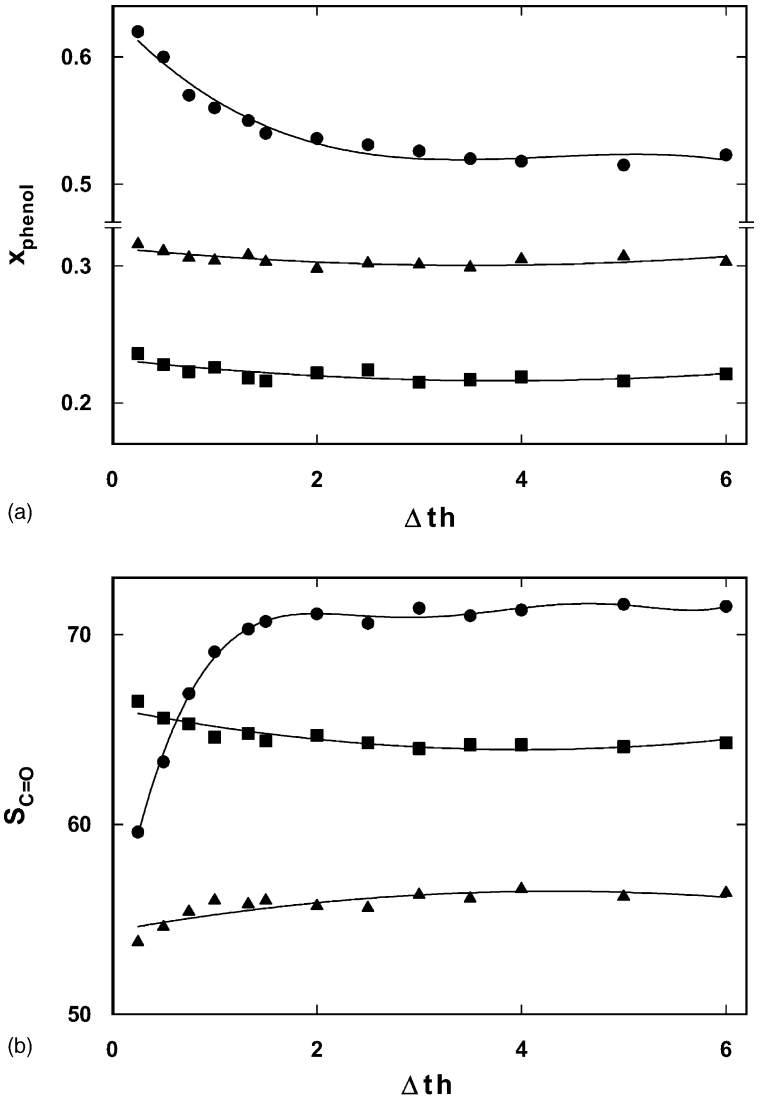

Fig. 4. Variation of (a) fractional phenol conversion (x_{phenol}) and (b) cyclohexanone selectivity ($S_{C=O}$) with time-on-stream over Pd/SiO_2-C (▲), Pd/SiO_2-III (■), and Pd–Yb/SiO_2-III (●): $T = 423$ K; $W/F_{phenol} = 128$ g mol h^{-1}.

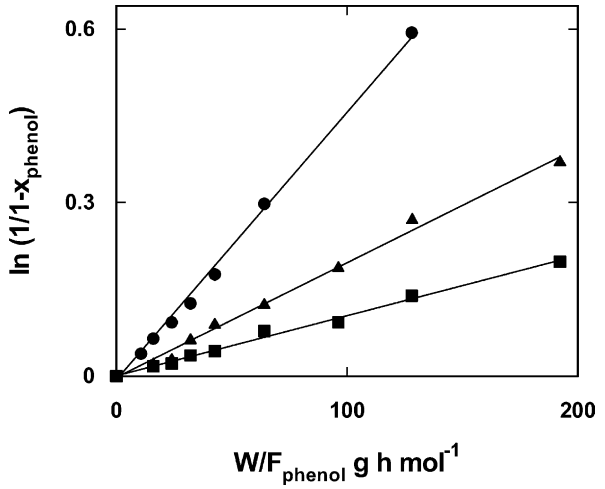

Fig. 5. Pseudo-first order kinetic relationships for the hydrogenation of phenol over Pd/SiO_2-C (▲), Pd/SiO_2-III (■), and Pd–Yb/SiO_2-III (●): $T = 448$ K.

to thermodynamic limitations [3,15] and/or a temperature induced decrease of the fraction of the catalyst surface that is covered by reactant(s) [8]. Thermochemical calculations have revealed that the gas phase equilibrium does exhibit a marked temperature dependence [7]. At the same inlet phenol partial pressure, complete conversion under equilibrium conditions is achieved at $T \leq 443$ K with a continual drop thereafter to a residual conversion at 573 K. The catalytic data generated in this study are far removed from gas phase equilibrium conversions and the response of activity to changes in temperature can be attributed positively to surface reaction phenomena. In the case of both monometallic Pd catalysts the activity temperature dependence was a function of Pd loading where the Pd dilute systems were less sensitive to temperature changes and the profiles for both nitrate and acetate-based catalysts coincided at a common % Pd, w/w. In marked contrast, incorporation of Yb on the surface ensured a consistently higher degree of

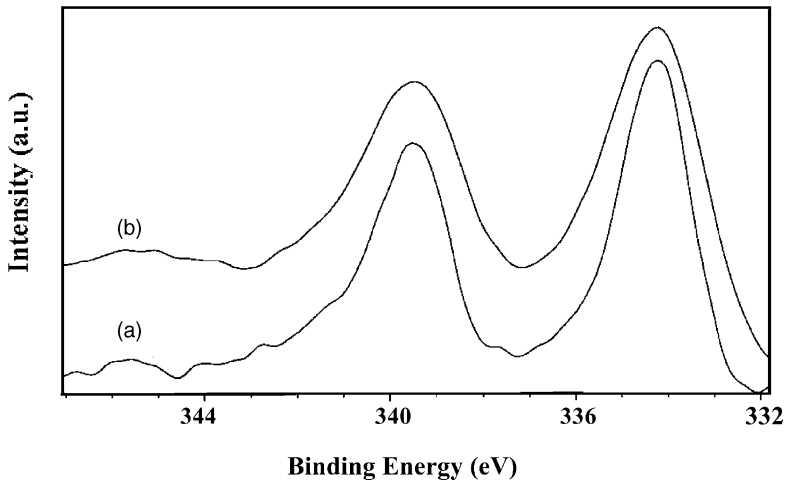

Fig. 6. XPS of (a) Pd/SiO_2-II and (b) $Pd–Yb/SiO_2$-II.

conversion that was largely maintained over the entire temperature interval, an effect that was common to all metal loadings.

Variations in reaction temperature also had a considerable effect on selectivity as can be seen from the relationship between conversion and cyclohexanone selectivity (at a fixed inlet molar feed rate) presented in Fig. 9. The lines provided are intended merely as a guide to aid visual assessment and do not possess any "fitting" significance. In contrast to the trends shown in Fig. 7, variations in temperature that result in increased phenol conversion also served to enhance the selectivity with which the partially hydrogenated cyclohexanone was produced. This response can be linked to temperature induced changes in the phenol/catalyst interaction(s) that are known to govern selectivity [17]. Taking the relationships plotted in Fig. 9, the predominant temperature related selectivity response can be flagged: the higher values of x_{phenol} were achieved with a decrease in reaction temperature (see Fig. 8) where stepwise hydrogenation must prevail with a higher associated cyclohexanone selectivity. A temperature induced desorption serves to lower x_{phenol} while a complete hydrogenation to cyclohexanol is favored.

The effect of incorporating Yb with Ni on phenol hydrogenation is considered in Table 2. There are clear cut differences in the catalytic behavior of Ni and Pd and, under the same reaction conditions, each Pd system was significantly more active than the Ni counterpart. It is, however, generally accepted that Pd-based catalysts are inherently more effective than Ni catalysts in promoting aromatic hydrogenation reactions [39]. The monometallic Ni/SiO_2 catalysts prepared from the nitrate and acetate precursors delivered comparable rate constants and cyclohexanone selectivities/yields. The presence of Yb again resulted in a

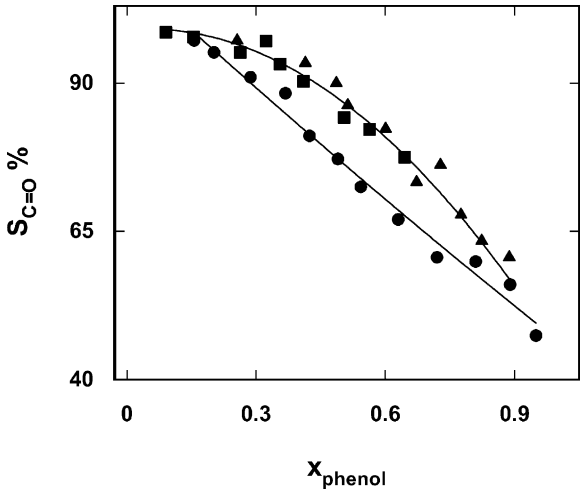

Fig. 7. Relationship between cyclohexanone selectivity ($S_{C=O}$) and fractional phenol conversion (x_{phenol}) over Pd/SiO_2 derived from nitrate (▲) and acetate (■) precursors and over $Pd–Yb/SiO_2$ (●) where W/F_{phenol} was varied and temperature was kept constant at 398 K.

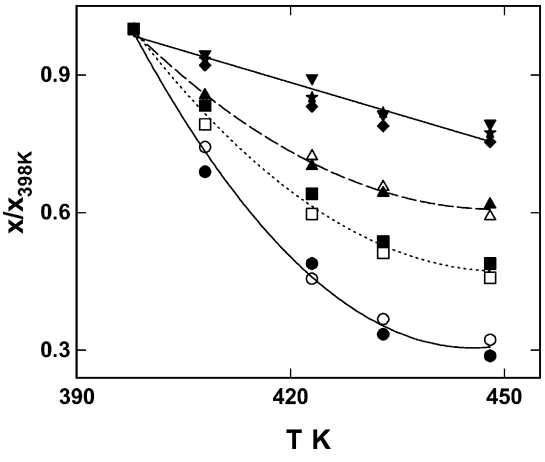

Fig. 8. Temperature dependence of the fractional phenol conversion (x) relative to that recorded at 398 K (x_{398K}) over 1% (w/w) (▲,△), 5% (w/w) (■,□) and 10% (w/w) (●,○) Pd/SiO_2 prepared from the nitrate (open symbols) and acetate (solid symbols) precursors and over $Pd–Yb/SiO_2$-I (▼),$Pd–Yb/SiO_2$-II (◆) and $Pd–Yb/SiO_2$-III (★): $W/F_{phenol} = 128\,g\,mol\,h^{-1}$.

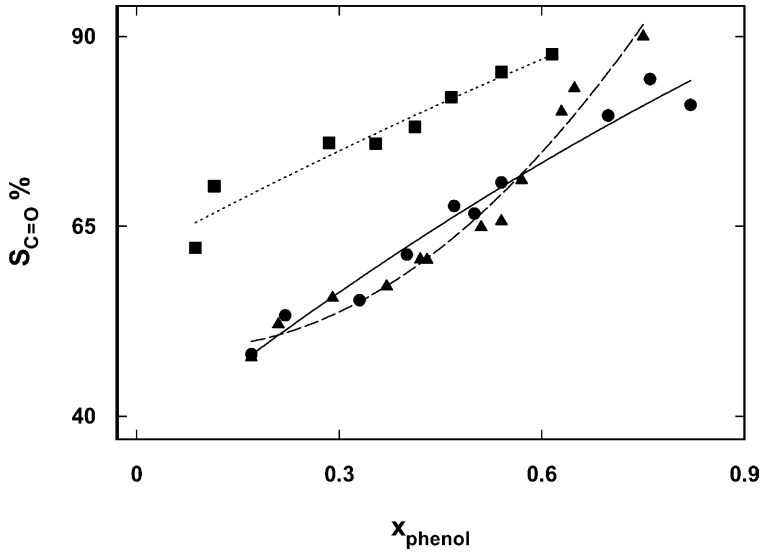

Fig. 9. Relationship between cyclohexanone selectivity ($S_{C=O}$) and fractional phenol conversion (x_{phenol}) over Pd/SiO_2 derived from nitrate (▲, dashed line $W/F_{phenol} = 128\,g\,mol\,h^{-1}$) and acetate (■, dotted line, $W/F_{phenol} = 43\,g\,mol\,h^{-1}$) precursors and over Pd–Yb/SiO_2 (●, solid line $W/F_{phenol} = 64\,g\,mol\,h^{-1}$) where the temperature was varied.

Table 2
Hydrogenation rate constant (k, per gram of transition metal), cyclohexanone selectivity ($S_{C=O}$) and yield ($Y_{C=O}$) associated with phenol conversion over Pd/SiO_2, Ni/SiO_2, Pd–Yb/SiO_2, and Ni–Yb/SiO_2 at 423 K where the Pd (or Ni) loading = 5% (w/w): $W/F_{phenol} = 128\,g\,mol^{-1}\,h$

	Nitrate precursor		Acetate precursor		Bimetallic	
	Pd/SiO_2	Ni/SiO_2	Pd/SiO_2	Ni/SiO_2	Pd–Yb/SiO_2	Ni–Yb/SiO_2
k ($\times 10^5$ mol h^{-1} g^{-1})	23	9	20	10	42	19
$S_{C=O}$ (%)	62	16	74	15	68	25
$Y_{C=O}$ (%)	27	3	25	4	47	15

significant enhancement of activity. Imamura et al. [40,41] have also noted an enhanced catalytic activity associated with Ni–Yb/SiO_2 when compared with Ni/SiO_2 in hydrogen transfer reactions involving ethane and buta-1,3-diene. The promotional effect of Yb in phenol hydrogenation extends to Ni on silica where the positive influence may again be ascribed to hydrogen transfer from the surface Yb hydride. In common with Pd–Yb/SiO_2, both phenol conversion and product distribution showed short-term temporal variations: the values given in Table 2 represent steady state conversion. While phenol conversion over Ni–Yb was greater than that recorded for both Ni/SiO_2 catalysts, the cyclohexanone selectivity was also greater resulting in a significant improvement (by over a factor of three) in cyclohexanone yield.

4. Conclusion

In the hydrogenation of phenol over Pd/SiO_2 and Pd–Yb/SiO_2, the presence of Yb has a significant impact on catalytic activity and selectivity. In the case of the supported monometallic Pd, use of palladium acetate or nitrate as the metal precursor has little effect on catalyst performance. The presence of Yb served to enhance phenol conversion, an effect that extends to silica supported Ni. A pseudo-first order kinetic analysis combined with TEM characterization has been used to deliver specific rate constants that were slightly lower for larger metal particles; the average Pd particle sizes spanned the range 2–8 nm for 1% to 10%, w/w Pd. While Yb/SiO_2 did not exhibit any hydrogenation activity the specific rates associated with the Pd–Yb bimetallic systems were appreciably greater than the monometallic Pd/SiO_2 at each Pd loading. This Pd–Yb synergistic effect is tentatively attributed to a greater availability of reactive hydrogen from surface Yb hydride species. The Yb component in Pd–Yb/SiO_2 is present as a thin coating with no evidence of distinct Yb particle formation or, on the basis of XPS analysis, disruption to the Pd site electron density. A decrease in the effective contact time lowered fractional conversion (over each catalyst) with a preferential formation of cyclohexanone. Where the contact time was maintained constant, an increase in reaction temperature lowered both conversion and cyclohexanone selectivity.

Acknowledgements

We are grateful to Gonzalo Pina for assistance with the catalysis measurements. This work was supported in

part by the National Science Foundation through Grant CTS-0218591 which MAK acknowledges. SGS also thanks the National Science Foundation for support through Grants CHE-9901115 and CHE-0213491.

References

[1] I. Dodgson, K. Griffen, G. Barberis, F. Pignatoro, G. Tauszik, Chem. Ind. (1989) 830.
[2] N. Mahata, K.V. Raghavan, V. Vishwanathan, C. Park, M.A. Keane, Phys. Chem. Chem. Phys. 3 (2001) 2712.
[3] G. Neri, A.M. Visco, A. Donato, C. Milone, M. Malentacchi, G. Gubitosa, Appl. Catal. A: General 110 (1994) 49.
[4] S. Narayanan, R. Unnikrishnan, J. Chem. Soc., Faraday Trans. 93 (1997) 2009.
[5] S. Narayanan, K. Krishna, Appl. Catal. A: General 147 (1996) L253.
[6] S. Narayanan, K. Krishna, Catal. Today 49 (1999) 57.
[7] P. Claus, H. Berndt, C. Mohr, J. Radnik, E.-J. Shin, M.A. Keane, J. Catal. 192 (2000) 88.
[8] S. Galvagno, A. Donato, G. Neri, R. Pietropaolo, J. Chem. Technol. Biotechnol. 51 (1991) 145.
[9] A.K. Talukdar, K.G. Bhattacharyya, S. Sivasanker, Appl. Catal. A: General 96 (1993) 229.
[10] N. Itoh, W.-C. Xu, Appl. Catal. A: General 107 (1993) 83.
[11] V. Vishwanathan, N. Mahata, M.A. Keane, React. Kinet. Catal. Lett. 72 (2001) 297.
[12] U.M. Tang, M.Y. Huang, Y.Y. Jiang, Macromol. Rapid Commun. 15 (1994) 527.
[13] M. Higashijima, S. Nishimura, Bull. Chem. Soc. Jpn. 64 (1992) 2955.
[14] S. Narayanan, G. Sreekanth, Ind. J. Technol. 31 (1993) 507.
[15] S. Narayanan, G. Sreekanth, React. Catal. Lett. 51 (1993) 449.
[16] E.-J. Shin, M.A. Keane, Ind. Eng. Chem. Res. 39 (2000) 883.
[17] E.-J. Shin, M.A. Keane, J. Catal. 173 (2000) 450.
[18] G. Pina, C. Louis, M.A. Keane, Phys. Chem. Chem. Phys. 5 (2003) 1924.
[19] Y.Z. Chen, C.W. Liaw, L.I. Lee, Appl. Catal A: General 177 (1999) 1.
[20] S.T. Srinivas, L.J. Lakshmi, P.K. Rao, Appl. Catal. A: General 110 (1994) 167.
[21] N. Mahata, V. Vishwanathan, Ind. J. Chem. 37A (1998) 652.
[22] S.G. Shore, E. Ding, C. Park, M.A. Keane, Catal. Commun. 3 (2002) 77.
[23] D.W. Knoeppel, J. Liu, E.A. Meyers, S.G. Shore, Inorg. Chem. 37 (1998) 4828.
[24] M.A. Armendia, V. Borau, I.M. Garcia, C. Jimenez, F. Lafont, A. Marinas, J.M. Marinas, F.J. Urbano, J. Catal. 187 (1999) 392.
[25] G. Tavoularis, M.A. Keane, J. Chem. Technol. Biotechnol. 74 (1999) 60.
[26] D.E. Mears, Ind. Eng. Chem. Proc. Des. Dev. 10 (1971) 541.
[27] JCPDS–ICDD, PCPDFWIN, Version 2.2, June (2001).
[28] A. Kern, W. Eysel,. Mineralogisch Petrograph, Univ. Heidelberg, 1993; CAS: 7440-05-3.
[29] F.L. Chen, Y. Sakamoto, T.B. Flanagan, Ber. Bunsen.-Gesell. Phys. Chem. Chem. Phys. 97 (1993) 784.
[30] A.E. Curzon, O. Singh, J. Phys. D: Appl. Phys. 8 (1975) 135.
[31] A.E. Curzon, O. Singh, J. Less Common Metals 39 (1975) 227.
[32] J.C. Warf, K.I. Hardcastle, Inorg. Chem. 5 (1966) 1736.
[33] J.C. Warf, K.I. Hardcastle, J. Am. Chem. Soc. 83 (1961) 2206.
[34] H. Imamura, Y. Maeda, T. Kumai, Y. Sakata, S. Tsuchiya, Catal. Lett. 88 (2003) 69.
[35] H. Imamura, K. Nishimura, T. Yoshimura, H. Yoshimochi, M. Ueno, Y. Sakata, S. Tsuchiya, J. Mol. Catal. A: Chemical 165 (2001) 189.
[36] H. Imamura, K. Igawa, Y. Kasuga, Y. Sakata, S. Tsuchiya, S. J. Chem. Soc., Faraday Trans. 90 (1994) 2119.
[37] H. Imamura, M. Suzuki, Y. Sakata, S. Tsuchiya, J. Alloy. Comp. 303 (2000) 514.
[38] V.M. Kuz'menko, A.N. Vladychkin, Phys. Solid State 41 (1999) 155.
[39] P.N. Rylander, Hydrogenation Methods, Academic Press, London, 1985.
[40] H. Imamura, Y. Miura, K. Fujita, Y. Sakata, S. Tsuchiya, J. Mol. Catal. A: Chemical 140 (1999) 81.
[41] H. Imamura, K. Fujita, Y. Miura, K. Mizuno, Y. Sakata, S. Tsuchiya, J. Chem. Soc., Chem. Commun. (1996) 1841.